energies

MDPI

Article

An Improved Multi-Timescale AEKF–AUKF Joint Algorithm for State-of-Charge Estimation of Lithium-Ion Batteries

Aihua Wu, Yan Zhou, Jingfeng Mao *, Xudong Zhang and Junqiang Zheng

School of Mechanical Engineering, Nantong University, Nantong 226019, China; wu.ah@ntu.edu.cn (A.W.); 2109320001@stmail.ntu.edu.cn (Y.Z.); zhang.xd69@ntu.edu.cn (X.Z.); zjq@ntu.edu.cn (J.Z.)
* Correspondence: mao.jf@ntu.edu.cn

Abstract: State-of-charge (SoC) estimation is one of the core functions of battery energy management systems. An accurate SoC estimation can guarantee the safe and reliable operation of the batteries system. In order to overcome the practical problems of low accuracy, noise uncertainty, poor robustness, and adaptability in parameter identification and SoC estimation of lithium-ion batteries, this paper proposes a joint estimation method based on the adaptive extended Kalman filter (AEKF) algorithm and the adaptive unscented Kalman filter (AUKF) algorithm in multiple time scales for 18,650 ternary lithium-ion batteries. Based on the slowly varying characteristics of lithium-ion batteries' parameters and the quickly varying characteristics of the SoC parameter, firstly, the AEKF algorithm was used to online identify the parameters of the model of batteries with a macroscopic time scale. Secondly, the identified parameters were applied to the AUKF algorithm for SoC estimation of lithium-ion batteries with a microscopic time scale. Finally, the comparative simulation experiments were implemented, and the experimental results show the proposed joint algorithm has higher accuracy, adaptivity, robustness, and self-correction capability compared with the conventional algorithm.

Keywords: SoC estimation; online parameter identification; adaptive unscented Kalman filter; adaptive extended Kalman filter; multiple time scales

Citation: Wu, A.; Zhou, Y.; Mao, J.; Zhang, X.; Zheng, J. An Improved Multi-Timescale AEKF–AUKF Joint Algorithm for State-of-Charge Estimation of Lithium-Ion Batteries. *Energies* **2023**, *16*, 6013. https://doi.org/10.3390/en16166013

Received: 26 July 2023
Revised: 4 August 2023
Accepted: 10 August 2023
Published: 17 August 2023

1. Introduction

Due to the gradual depletion of fossil fuels and increasing environmental pollution caused by the widespread use of fuel-powered vehicles, electric vehicles have received increasing attention due to their advantages in energy conservation and environmental protection. Currently, lithium batteries are the main energy source for electric vehicles. Their SoC parameter is one of the most basic and critical parameters in the energy management of batteries and vehicle power distribution [1,2].

At present, scholars have studied various SoC estimation algorithms, the most commonly used being the open-circuit voltage algorithm, the ampere-hour integration algorithm, and the model-based algorithm. The open-circuit voltage algorithm requires a longer charging time, which is not suitable for practical engineering [3]. The accuracy of the ampere-hour integration algorithm is closely related to the selection of the initial value, and due to the operation of the integration, it will continuously generate accumulated errors [4]. The model-based algorithm is divided into three categories. One is the black-box model algorithm, such as the neural network method [5] and the support vector machine method [6]. These methods require a large amount of training data, and the generalization ability of the models are poor. The second is the electrochemical model method, which can accurately describe the changes inside the batteries, but the computational complexity is high. The third is the equivalent circuit model method, which combines the equivalent circuit model with the filtering algorithm; the computation is small and the robustness is good, but it has a high demand for the model accuracy [7].

In recent years, scholars have conducted extensive research on parameter identification and SoC estimation algorithms for equivalent circuit models of lithium-ion batteries.

Online parameter identification can reflect the state changes of the batteries in real time, and compared with offline estimation algorithm, it does not need to collect a large amount of data offline, thus saving experimental time and cost [8]. The Kalman filter (KF) theory is a classical optimal filtering theory that adopts a time-domain state–space approach. It introduces the concept of a state space and utilizes the state equation of a linear system to perform optimal estimation of the system's state based on the input and output observation data. The KF algorithm, guided by the principle of minimum mean square error, can provide optimal estimation for complex, dynamic systems and has been widely applied in parameter identification and state of charge (SoC) estimation of lithium-ion batteries; however, the KF algorithm is only applicable to linear systems and is not suitable for nonlinear systems. Consequently, scholars have started researching corresponding improved algorithms. Yang et al. [9] proposed an extended Kalman filter (EKF) algorithm based on a first-order RC model and optimized it through piecewise fitting. The accuracy of the optimized EKF algorithm was significantly improved. Miao et al. [10] proposed an adaptive fractional-order unscented Kalman filter (UKF) that addresses the issue of unknown parameters and order, thereby enhancing the precision of SoC estimation. Ma et al. [11] introduced a cubature Kalman filter (CKF) algorithm based on the generalized maximum correlation coefficient criterion. The results show that compared to the traditional KF algorithm, the proposed CKF algorithm is capable of accurately estimating the SoC of lithium-ion batteries under non-Gaussian noise interference considering different temperatures and operating conditions. Currently, most derived algorithms of the KF algorithm are combined with other advanced algorithms. Zhu et al. [12] proposed a co-estimation algorithm that employs recursive restricted total least squares to identify the model parameters, and unscented Kalman filter (UKF) to estimate the SoC parameter, which improved the identification accuracy of the model parameters, but the UKF algorithm could not effectively filter out the noise. Ge et al. [13] proposed an improved forgetting factor recursive least squares (FFRLS) based on dynamic constraint and parameter backtracking, and combined it with the extended Kalman filter algorithm (EKF) to estimate the SoC parameter of lithium-ion batteries, achieving high estimation accuracy; however, the complexity of the algorithm is high, the computational effort is large, and the noise variance has to be set as a constant in the EKF algorithm. Wu et al. [14] proposed an adaptive EKF algorithm based on the maximum correlation entropy criterion (MCC-AEKF), which uses the maximum correlation entropy criterion to obtain accurate SoC estimation results. By replacing the overall solution with the local optimal solution, the algorithm has high accuracy and adaptability for SoC estimation, but has strong dependence on the model. Liu et al. [15] proposed an online parameter estimation using the FFRLS algorithm and the adaptive unscented Kalman filter (AUKF) algorithm for SoC estimation, which has strong robustness to external disturbances.

There are multiple time constants in the electrochemical reactions and transport processes of lithium-ion batteries, which lead to the dynamic characteristics of lithium-ion batteries exhibiting different characteristics at different time scales; therefore, some scholars have started to study improved algorithms for the SoC estimation of batteries at different time scales. Xiong et al. [16] proposed a dual extended Kalman filter algorithm (DEKF) considering multiple time scales for online parameter identification and joint SoC estimation of batteries, which greatly improved the applicability of the model for complex operating conditions. Despite this, the EKF algorithm ignored some of the higher order terms when linearizing the nonlinear system, which, in turn, led to a certain number of errors. Ji et al. [17] proposed a multi-scale multi-innovation unscented Kalman filter and extended Kalman filter (MIUKF-EKF) joint algorithm. They used the EKF algorithm for parameter identification at the macro time scale and used MIUKF to estimate the batteries' SoC at the micro-time scale, ensuring the accuracy of the SoC estimation and improving the computational efficiency; however, it cannot perform real-time correction of noise variance. Feng et al. [18] proposed a multi-time scale and capacity-based passive equalizer lithium-ion batteries pack equalization strategy, which uses a double extended Kalman filter and the minimum capacity difference model (MCDM) to estimate the SoC and capacity of the

battery pack in multiple time scales. This method can efficiently and accurately estimate the SoC and capacity of new and old batteries and improve the calculation efficiency and accuracy of the minimum capacity cell and batteries pack. Although the algorithms above have made further progress in the parameter identification and SoC estimation of lithium-ion batteries, they fail to provide a comprehensive consideration in terms of the hardware computation volume, time variability of the batteries and uncertainty of noise.

In response to the advantages and disadvantages of the research in parameter identification and SoC estimation of lithium batteries discussed above, and considering the characteristics of slow changes in battery model parameters over time and rapid changes in SoC over time, this paper proposes an improved multi-time scale algorithm. That is, at the macroscopic time scale, the AEKF algorithm is used to identify the parameters of the battery equivalent circuit model online, and at the microscopic time scale, the AUKF algorithm is used to estimate the SoC of lithium batteries.

This work is organized as follows: Section 1 introduces the definition of batteries' SoC and establishes the second-order *RC* equivalent circuit model for lithium-ion batteries. Section 2 presents the traditional EKF algorithm and UKF algorithm, and the proposed multi-timescale AEKF–AUKF joint algorithm with an implementation flowchart. Section 3 demonstrates the online identification of the model parameters of the lithium-ion batteries, and then compares and analyzes the identification accuracy of the EKF algorithm with that of the AEKF algorithm. Section 4 analyzes the accuracy of the proposed multi-timescale AEKF–AUKF joint algorithm for lithium-ion batteries' SoC estimation, setting up three cases for comparison and analysis. Section 5 summarizes the work and research results of this paper.

2. Lithium-Ion Batteries Modelling

2.1. Definition of SoC

The batteries' SoC represents the ratio of its remaining capacity after a period of use or long period of inactivity to the maximum available capacity. It can be expressed as [19]

$$SoC = \frac{C_t}{C_N} \times 100\%, \tag{1}$$

where C_t represents the remaining capacity of the batteries and C_N represents the maximum available capacity of the batteries.

In practical applications, in order to better simulate the batteries' actual operating conditions, the following equation is often used to define the SoC based on multiple time scales.

$$SoC_{k,l} = SoC_{0,0} - \frac{1}{C_N} \int_{t_{0,0}}^{t_{k,l}} \eta I_\tau d\tau, \tag{2}$$

where $k, l \in [1, L]$ are the time-scale indicators of the system parameters at the macroscopic time scale and the microscopic time scale, respectively, and L is the indicator defining the two time scales; $SoC_{k,l}$ is the SoC value at time $t_{k,l}$, and $SoC_{0,0}$ is the initial value of the batteries' SoC; I_τ is the current value of the batteries at time τ (positive for the discharge current and negative for the charge current); and η is the coulombic efficiency, which is a function of temperature and current.

The discrete-time of Equation (2) above can be expressed as

$$SoC_{k,l} = SoC_{k,l-1} - \frac{\eta \Delta t I_{k,l-1}}{C_N}. \tag{3}$$

where $SoC_{k,l-1}$ is the SoC value at time $t_{k,l-1}$, Δt is the sampling interval between two adjacent measurement points, and $I_{k,l-1}$ is the current value of the batteries at time $t_{k,l-1}$.

2.2. Equivalent Circuit Model

In order to improve the accuracy of the SoC estimation of lithium-ion batteries, a suitable equivalent circuit model that can more intuitively describe the influencing factors and operating characteristics of the batteries needs to be selected. In this study, the second-order *RC* equivalent circuit model was chosen, as shown in Figure 1. The *RC* circuit describes the polarization characteristics of the batteries during charging and discharging.

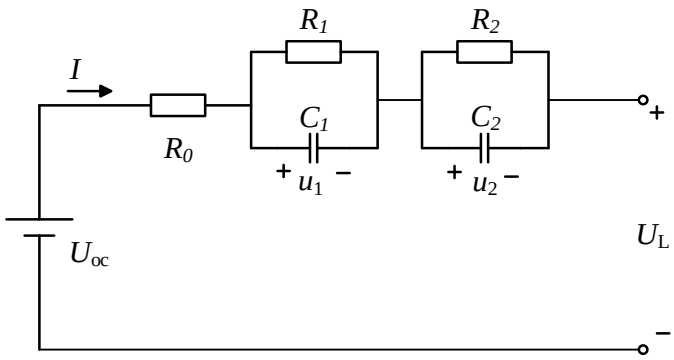

Figure 1. Second-order *RC* equivalent circuit model of lithium-ion batteries.

The electrical characteristics of the second-order *RC* equivalent circuit model can be expressed as

$$\begin{cases} U_L = U_{oc} - u_1 - u_2 - IR_0 \\ \dot{u}_1 = -\frac{1}{R_1C_1}u_1 + \frac{1}{C_1}I \\ \dot{u}_2 = -\frac{1}{R_2C_2}u_2 + \frac{1}{C_2}I \end{cases} . \quad (4)$$

where U_{oc} is the open circuit voltage of the lithium-ion batteries; I is its input current; u_1 and u_2 are the polarization voltages on the two *RC* networks, respectively; $\dot{u}_1$ and $\dot{u}_2$ are the first order derivatives of the polarization voltages u_1 and u_2, respectively; R_0 is the internal resistance; R_1 and R_2 are the polarization resistances; and C_1 and C_2 are the polarization capacitances. Among them, the *RC* circuit composed of R_1 and C_1 mainly describes the electrochemical reaction process of ions gaining and losing electrons, while the *RC* circuit composed of R_2 and C_2 mainly describes the diffusion of ions in the electrolyte.

According to the slowly varying characteristics of lithium-ion batteries parameters and the quickly varying characteristics of the batteries' state, a multi-timescale algorithm is used to construct the state–space equations, which predict the system parameter and the system state on macroscopic and microscopic timescales, respectively. The state–space equations can be expressed as

$$\begin{cases} \theta_{k+1} = \theta_k + \rho_k \\ x_{k,l+1} = f(x_{k,l}, \theta_k, u_{k,l}) + w_{k,l} \\ y_{k,l} = g(x_{k,l}, \theta_k, u_{k,l}) + v_{k,l} \end{cases} . \quad (5)$$

where $x_{k,l}$ is the system state matrix at time $t_{k,l} = t_{k,0} + l\Delta t$; $u_{k,l}$ is the input variable of the system at the time $t_{k,l}$, which is the input current of the lithium-ion batteries; θ_k is the system parameter matrix at time k, $\theta = [R_0\ R_1\ C_1\ R_2\ C_2]$; $y_{k,l}$ is the observation value at time $t_{k,l}$, and it is the terminal voltage of the lithium-ion batteries; $w_{k,l}$ and ρ_k are the process noise of the system state and system parameter, respectively; and $v_{k,l}$ is the observation noise of the system at time $t_{k,l}$. Both the process noise and observation noise are uncorrelated Gaussian white noise obeying Gaussian normal distribution. The variance matrix of the system parameter process noise ρ_k is $M_k = E(\rho_k\rho_k^T)$, the variance matrix of the system state process noise w_k is $Q_k = E(w_kw_k^T)$, and the variance matrix of the system observation noise v_k is $R_k = E(v_kv_k^T)$.

For the second-order *RC* equivalent circuit model in Figure 2, the discrete-time state Equation (6) and the observation Equation (7) of the batteries are obtained from Equations (3) and (4) based on the batteries' characteristics.

$$x_{k,l+1} = \begin{pmatrix} SoC_{k,l+1} \\ u^1_{k,l+1} \\ u^2_{k,l+1} \end{pmatrix} = \begin{pmatrix} 1 & 0 & 0 \\ 0 & e^{-\frac{\Delta t}{\tau_1}} & 0 \\ 0 & 0 & e^{-\frac{\Delta t}{\tau_2}} \end{pmatrix} \begin{pmatrix} SoC_{k,l} \\ u^1_{k,l} \\ u^2_{k,l} \end{pmatrix} + \begin{pmatrix} \frac{-\eta \Delta t}{C_N} \\ R_1\left(1 - e^{-\frac{\Delta t}{\tau_1}}\right) \\ R_2\left(1 - e^{-\frac{\Delta t}{\tau_2}}\right) \end{pmatrix} I_{k,l} + \begin{pmatrix} w_{1_{k,l}} \\ w_{2_{k,l}} \\ w_{3_{k,l}} \end{pmatrix}, \quad (6)$$

$$y_{k,l} = U_{oc}(SoC_{k,l}) - I_{k,l}R_0 - u^1_{k,l} - u^2_{k,l} + v_{k,l}, \quad (7)$$

where $x_{k,l+1}$ is the state variable of the system at time $t_{k,l+1}$, which contains the $SoC_{k,l+1}$ of the lithium-ion batteries at time $t_{k,l+1}$, polarization voltage $u^1_{k,l+1}$ and $u^2_{k,l+1}$; τ_1 and τ_2 are the time constants, $\tau_1 = R_1C_1$ and $\tau_2 = R_2C_2$; $I_{k,l}$ is the input current of the lithium-ion batteries at time $t_{k,l}$; U_{oc} ($SoC_{k,l}$) is the corresponding open circuit voltage of the system at time $t_{k,l}$, which is a function according to SoC; and $w_{1_{k,l}}$, $w_{2_{k,l}}$, and $w_{3_{k,l}}$ are the process noise matrices of the system state, respectively.

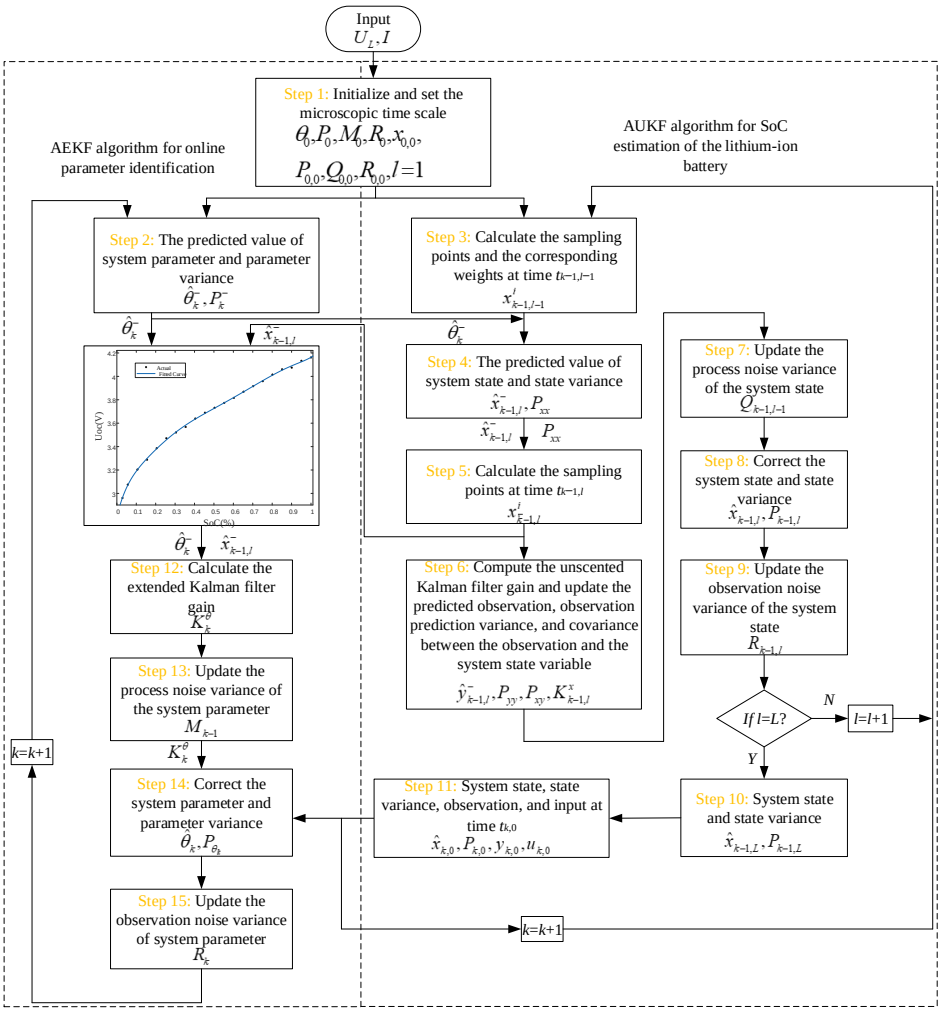

Figure 2. Flow chart of the multi-timescale AEKF–AUKF joint algorithm.

The function $f(x_{k,l},\ \theta_k,\ u_{k,l})$ and the function $g(x_{k,l},\ \theta_k,\ u_{k,l})$ in Equation (5) can be expressed as

$$\begin{cases} f(x_{k,l},\theta_k,u_{k,l}) = \begin{pmatrix} 1 & 0 & 0 \\ 0 & e^{-\frac{\Delta t}{\tau_1}} & 0 \\ 0 & 0 & e^{-\frac{\Delta t}{\tau_2}} \end{pmatrix} \begin{pmatrix} SoC_{k,l} \\ u^1_{k,l} \\ u^2_{k,l} \end{pmatrix} + \begin{pmatrix} \frac{-\eta\Delta t}{C_N} \\ R_1\left(1-e^{-\frac{\Delta t}{\tau_1}}\right) \\ R_2\left(1-e^{-\frac{\Delta t}{\tau_2}}\right) \end{pmatrix} I_{k,l} \\ g(x_{k,l},\theta_k,u_{k,l}) = U_{oc}(SoC_{k,l}) - I_{k,l}R_0 - u^1_{k,l} - u^2_{k,l} \end{cases} . \quad (8)$$

3. Multi-Timescale AEKF–AUKF Joint Algorithm

In this section, firstly, according to Equation (5), the traditional EKF algorithm and UKF algorithm are introduced at multiple time scales, which have achieved remarkable results in parameter identification and SoC estimation of batteries. Then, based on these two traditional algorithms, a multi-time scale AEKF–AUKF joint algorithm is constructed to improve the parameter identification and SoC estimation accuracy, making the estimation results more reliable.

3.1. Principle of the EKF Algorithm

The traditional Kalman filter theory is only effective for linear models; however, most of the practical applications are nonlinear models. In order to make the Kalman filter algorithm applicable to nonlinear systems, the extended Kalman filter algorithm (EKF) is proposed. The EKF algorithm can linearize nonlinear systems by performing a first-order Taylor expansion on the nonlinear functions in the system and neglecting the higher-order terms above the second order, thereby approximating the nonlinear system as a linear system. The main steps of the recursive equations of the EKF algorithm are as follows [20].

Step 1: Initialize system parameter θ_0 and parameter variance matrix P_{θ_0}.

$$\theta_0 = E(\theta_0), \quad (9)$$

$$P_{\theta_0} = E\left[(\theta_0 - \hat{\theta}_0)(\theta_0 - \hat{\theta}_0)^T\right] \quad (10)$$

Step 2: Obtain the predicted value of system parameter $\hat{\theta}_k^-$ at time k.

The predicted value of the system parameter $\hat{\theta}_k^-$ at time k is obtained from the optimal estimate value of the system parameter $\hat{\theta}_{k-1}$ at time $k-1$.

$$\hat{\theta}_k^- = \hat{\theta}_{k-1}. \quad (11)$$

Step 3: Obtain the parameter prediction variance matrix $P_{\theta_k}^-$ at time k.

The parameter prediction variance matrix $P_{\theta_k}^-$ at time k is calculated on the basis of the parameter optimal estimation variance matrix $P_{\theta_{k-1}}$ at time $k-1$, and the variance matrix M_{k-1} of the process noise at time $k-1$.

$$P_{\theta_k}^- = P_{\theta_{k-1}} + M_{k-1}. \quad (12)$$

Step 4: Correct the gain matrix K_k^θ of the extended Kalman filter.

The extended Kalman filter gain matrix K_k^θ at time k is calculated on the basis of the parameter prediction variance matrix $P_{\theta_k}^-$, the observation matrix C_k^θ at time k, and the variance matrix R_k of the observation noise at time k.

$$K_k^\theta = \frac{P_{\theta_k}^-\left(C_k^\theta\right)^T}{C_k^\theta P_{\theta_k}^-\left(C_k^\theta\right)^T + R_k} \quad (13)$$

where C_k^θ is expressed as [21]

$$\begin{aligned} C_k^\theta &= \frac{dg\left(\hat{x}_{k,0},\theta,u_{k,0}\right)}{d\theta}\Big|\theta=\hat{\theta}_k^- \\ &= \frac{\partial g\left(\hat{x}_{k,0},\hat{\theta}_k^-,u_{k,0}\right)}{\partial\hat{\theta}_k^-} + \frac{\partial g\left(\hat{x}_{k,0},\hat{\theta}_k^-,u_{k,0}\right)}{\partial\hat{x}_{k,0}} \times \frac{d\hat{x}_{k,0}}{d\hat{\theta}_k^-}. \end{aligned} \tag{14}$$

Step 5: Correct the predicted value of the system parameter $\hat{\theta}_k^-$.

Correct the predicted value of the system parameter $\hat{\theta}_k^-$ according to the extended Kalman filter gain matrix K_k^θ at time k to obtain the optimal estimated value of the system parameter $\hat{\theta}_k$ at time k.

$$\hat{\theta}_k = \hat{\theta}_k^- + K_k^\theta\left(y_{k,l} - g\left(\hat{x}_{k,l},\hat{\theta}_k^-,u_{k,l}\right)\right). \tag{15}$$

Step 6: Correct the parameter prediction variance matrix P_{θ_k}.

Based on the extended Kalman filter gain matrix K_k^θ and the observation matrix C_k^θ at time k, the parameter prediction variance matrix $P_{\theta_k}^-$ is corrected, and then the parameter optimal estimation variance matrix P_{θ_k} at time k is obtained [22].

$$P_{\theta_k} = \left(I - K_k^\theta C_k^\theta\right)P_{\theta_k}^-. \tag{16}$$

Step 7: The corrected optimal estimation of the system parameter $\hat{\theta}_k$ is used as the initial value of the system parameter for the next recurrence, and the above steps 1 to 6 are repeated until a more accurate estimation result is obtained. The estimation results can be used for both the parameter identification and the SoC estimation of the batteries.

3.2. Principle of the UKF Algorithm

Since the EKF algorithm ignores higher-order terms above the second order when linearizing nonlinear systems, it inevitably led to an increase in the estimation error; therefore, the unscented Kalman filter (UKF) algorithm based on certain regular sampling is proposed [23].

The UKF algorithm constructs probability density distributions for the sigma sampling points obtained from the unscented transform, approximating polynomials consisting of constant, first-order, and higher-order terms in the nonlinear equation, which satisfies the nonlinearity condition and enables fast and accurate prediction updates.

The basic principle of unscented transform is as follows: sigma point set extraction is carried out near the estimated value under the condition that the mean and variance are unchanged. Then, obtain the new mean and variance. Next, place the extraction point x and weight values ω into Equation (5), and obtain the corrected nonlinear acquisition point. The steps for the extraction points and weights are as follows.

Step 1: For an n-dimensional state variable x, construct the set of $2n + 1$ sigma points $x_{k-1,l-1}^i$, $i = 0, 1,..., 2n$.

$$x_{k-1,l-1}^i = \begin{cases} \hat{x}_{k-1,l-1} & ,i=0 \\ \hat{x}_{k-1,l-1} + \left(\sqrt{(n+\lambda)P_{k-1,l-1}}\right)_i, & i=1,2,\cdots,n \\ \hat{x}_{k-1,l-1} - \left(\sqrt{(n+\lambda)P_{k-1,l-1}}\right)_i, & i=n+1,\cdots,2n \end{cases} \tag{17}$$

where n is the dimensionality of the state variable x; the superscript i indicates the number of points selected for sampling; $P_{k-1,l-1}$ is the variance of the sampled points at time $t_{k-1,l-1}$; $\left(\sqrt{(n+\lambda)P_{k-1,l-1}}\right)_i$ is the ith column of the matrix; and λ is the scaling parameter, which determines the final prediction result error. λ can be expressed as [24]

$$\lambda = \alpha^2(n+\kappa) - n \tag{18}$$

where α is the modulation factor of the density distribution of the sampling points and κ is a secondary parameter that determines the prediction accuracy.

Step 2: Calculate the weights ω corresponding to the sigma sampling points.

$$\begin{cases} \omega_m^0 = \frac{\lambda}{n+\lambda}, i = 0 \\ \omega_c^0 = \frac{\lambda}{n+\lambda} + \left(1 - \alpha^2 + \beta\right), i = 0 \\ \omega_m^i = \omega_c^i = \frac{1}{2(n+\lambda)}, i = 1, 2, \ldots, 2n \end{cases} \tag{19}$$

where the subscripts m and c are the mean and variance, respectively, and β is the state scatter adjustment value, usually, $\beta = 2$.

The UKF algorithm consists mainly of system initialization and state prediction and correction [25], as described in the following steps.

Step 1: Initialize system state $x_{0,0}$ and state variance matrix $P_{0,0}$.

$$x_{0,0} = E(x_{0,0}), \tag{20}$$

$$P_{0,0} = E\left[(x_{0,0} - \hat{x}_{0,0})(x_{0,0} - \hat{x}_{0,0})^T\right] \tag{21}$$

Step 2: Use Equations (17) and (19) to perform the unscented transformation, and construct the set of $2n + 1$ sigma points $x_{k-1,l-1}^i$, $i = 0, 1, \ldots, 2n$, based on the system state $\hat{x}_{k-1,l-1}$ and the state variance matrix $P_{k-1,l-1}$ at time $t_{k-1,l-1}$.

$$x_{k-1,l-1}^i = \left(\hat{x}_{k-1,l-1}, \hat{x}_{k-1,l-1} + \sqrt{(n+\lambda)P_{k-1,l-1}}, \hat{x}_{k-1,l-1} - \sqrt{(n+\lambda)P_{k-1,l-1}}\right). \tag{22}$$

Step 3: Substitute Equation (22) into the nonlinear function f of Equation (5), then obtain the $2n + 1$ sigma points at time $t_{k-1,l}$ after the unscented transformation of the system state $x_{\bar{k}-1,l}^i$.

$$x_{\bar{k}-1,l}^i = f\left(x_{k-1,l-1}^i, \hat{\theta}_k^-, u_{k-1,l-1}\right). \tag{23}$$

Step 4: Using Equation (23) and the weights of Equation (19), update the predicted value of the system state $\hat{x}_{k-1,l}^-$ and the state prediction variance matrix P_{xx} at time $t_{k-1,l}$ [26].

$$\hat{x}_{k-1,l}^- = \sum_{i=0}^{2n} \omega_m^i x_{\bar{k}-1,l}^i, \tag{24}$$

$$P_{xx} = \sum_{i=0}^{2n} \omega_c^i \left[x_{\bar{k}-1,l}^i - \hat{x}_{k-1,l}^-\right]\left[x_{\bar{k}-1,l}^i - \hat{x}_{k-1,l}^-\right]^T + Q_{k-1,l-1} \tag{25}$$

Step 5: Based on Equations (24) and (25), the new sigma point set is obtained again using the unscented transformation $x_{\bar{k}-1,l}^i$.

$$x_{\bar{k}-1,l}^i = \left(\hat{x}_{k-1,l}^-, \hat{x}_{k-1,l}^- + \sqrt{(n+\lambda)P_{xx}}, \hat{x}_{k-1,l}^- - \sqrt{(n+\lambda)P_{xx}}\right). \tag{26}$$

Step 6: Substitute Equation (26) into the nonlinear function g of Equation (5), and then obtain the sigma point $y_{\bar{k}-1,l}^i$ at time $t_{k-1,l}$ after the second unscented transformation of the system observation value.

$$y_{\bar{k}-1,l}^i = g\left(x_{\bar{k}-1,l}^i, \hat{\theta}_k^-, u_{k-1,l}\right). \tag{27}$$

Step 7: Using Equations (19) and (27), update the system predicted observation $\hat{y}_{k-1,l}^-$, the observation prediction variance matrix P_{yy}, and the covariance matrix P_{yy} between the system state variable and the observation [27].

$$\hat{y}_{k-1,l}^- = \sum_{i=0}^{2n} \omega_m^i y_{\bar{k}-1,l}^i, \tag{28}$$

$$P_{yy} = \sum_{i=0}^{2n} \omega_c^i \left[y_{k-1,l}^i - \hat{y}_{k-1,l}^- \right] \left[y_{k-1,l}^i - \hat{y}_{k-1,l}^- \right]^T + R_{k-1,l}, \tag{29}$$

$$P_{xy} = \sum_{i=0}^{2n} \omega_c^i \left[x_{k-1,l}^i - \hat{x}_{k-1,l}^- \right] \left[y_{k-1,l}^i - \hat{y}_{k-1,l}^- \right]^T \tag{30}$$

Step 8: Using Equations (29) and (30), calculate the unscented Kalman filter gain matrix $K_{k-1,l}^x$ at time $t_{k-1,l}$.

$$K_{k-1,l}^x = P_{xy} \left(P_{yy} \right)^{-1}. \tag{31}$$

Step 9: From the unscented Kalman filter gain matrix, system state, observation value, and covariance matrix at time $t_{k-1,l}$, obtain the corrected optimal estimation of the system state $\hat{x}_{k-1,l}$ and the state optimal estimation variance matrix $P_{k-1,l}$.

$$\hat{x}_{k-1,l} = \hat{x}_{k-1,l}^- + K_{k-1,l}^x \left(y_{k-1,l} - \hat{y}_{k-1,l}^- \right), \tag{32}$$

$$P_{k-1,l} = P_{xx} - K_{k-1,l}^x P_{xy}^T. \tag{33}$$

Step 10: Take the corrected optimal estimation of the system state $\hat{x}_{k-1,l}$ as the initial value of the system state for the next recurrence, and steps 1 to 9 above are repeated until a more accurate estimation result is obtained. The estimation results can be used for both the parameter identification and the SoC estimation of the batteries.

Although the UKF algorithm does not require a linearization transformation for the nonlinear system compared to the EKF algorithm, there is still a weight between the UKF algorithm and the EKF algorithm. When using Taylor's formula to expand the equations, the EKF algorithm ignores higher-order terms, which can lead to inaccurate estimation results. The UKF algorithm, which uses the unscented transformation to transform an approximately linear function into a probability density function, is more accurate than the EKF algorithm; however, the UKF algorithm is more computationally intensive and slower to calculate, and the noise variance in the UKF algorithm is determined by empirical choices, which can lead to biased filtering results [28,29].

3.3. Design of the Multi-Timescale AEKF–AUKF Joint Algorithm

In the traditional filtering algorithms mentioned above, the noise variance matrix is treated as a constant; however, in practical applications, the noise is not always fixed and may not necessarily be Gaussian white noise. This will cause the estimation results of traditional algorithms to be affected by system noise and uncertainty, leading to inevitable errors in system estimation.

To improve the accuracy of the parameter identification and SoC estimation results for lithium-ion batteries, a multi-timescale joint algorithm is proposed. The AEKF algorithm is used for online parameter identification at the macroscopic time scale, and the AUKF algorithm is used for SoC estimation at the microscopic time scale.

The steps of the multi-timescale AEKF–AUKF joint algorithm are as follows:

Step 1: Initialize the system parameter θ_0, the parameter variance matrix P_{θ_0}, the system state $x_{0,0}$, and the state variance matrix $P_{0,0}$, as in Equations (9), (10), (20) and (21).

Step 2: Update the system parameter and the parameter variance matrix at the macroscopic time scale k using Equations (11) and (12).

Step 3: Sigma point set extraction for the system state variable at time $t_{k-1,l-1}$ at the microscopic time scale l, and calculate the corresponding weight values by Equations (19) and (22).

Step 4: Calculate the predicted value of the system state and the state prediction variance matrix with Equations (24) and (25).

Step 5: Sigma point set extraction for the system state variable at time $t_{k-1,l}$ using the unscented transformation with Equation (26);

Step 6: Calculate the unscented Kalman filter gain matrix at time $t_{k-1,l}$, and update the predicted observation, the observation prediction variance matrix, and the covariance matrix between the system state variable and the observation using Equations (28)–(31).

Step 7: Introduce an innovation value based on the terminal voltage error of the lithium-ion batteries, and perform an adaptive update of the process noise variance matrix of the system state [30].

The innovation value is the error between the actual observation $y_{k-1,l}$ and the predicted observation $\hat{y}^-_{k-1,l}$, denoted as

$$\begin{aligned} m_{k-1,l} &= y_{k-1,l} - \hat{y}^-_{k-1,l} \\ &= y_{k-1,l} - g\left(\hat{x}^-_{k-1,l}, \hat{\theta}^-_k, u_{k-1,l}\right) \end{aligned} \tag{34}$$

Calculate the real-time estimated variance value of the innovation.

$$G_{m_{k-1,l}} = \begin{cases} \frac{k-1}{k} G_{m_{k-1,l-1}} + \frac{1}{k} m_{k-1,l} m^T_{k-1,l} & k \le N \\ \frac{1}{N} \sum\limits_{q=k-N+1}^{k} m_{q,l} m^T_{q,l} & k > N' \end{cases} \tag{35}$$

where N is the moving window size and $m_{q,l}$ is an element value of $m_{k-1,l}$ in the range $q = k - N + 1$ to k.

The process noise variance matrix of the system state is updated with the real-time estimated variance value of the innovation, denoted as

$$Q_{k-1,l-1} = K^x_{k-1,l} G_{m_{k-1,l}} \left(K^x_{k-1,l}\right)^T. \tag{36}$$

Step 8: Correct the system state and state variance matrix by Equations (32) and (33).

Step 9: Introduce a residual value based on the terminal voltage error of the lithium-ion batteries, and perform an adaptive update of the observed noise variance matrix of the system state [31].

The residual value is the error between the actual observation $y_{k-1,l}$ and the filtered estimated observation $\hat{y}_{k-1,l}$, denoted as

$$\begin{aligned} r_{k-1,l} &= y_{k-1,l} - \hat{y}_{k-1,l} \\ &= y_{k-1,l} - g\left(\hat{x}_{k-1,l}, \hat{\theta}^-_k, u_{k-1,l}\right) \end{aligned} \tag{37}$$

Calculate the real-time estimated variance value of the residual.

$$G_{r_{k-1,l}} = \begin{cases} \frac{k-1}{k} G_{r_{k-1,l-1}} + \frac{1}{k} r_{k-1,l} r^T_{k-1,l} & k \le N \\ \frac{1}{N} \sum\limits_{q=k-N+1}^{k} r_{q,l} r^T_{q,l} & k > N' \end{cases} \tag{38}$$

where $r_{q,l}$ is an element value of $r_{k-1,l}$ in the range $q = k - N + 1$ to k.

The observed noise variance matrix of the system state is updated with the real-time estimated variance value of the residual, denoted as

$$R_{k-1,l} = G_{r_{k-1,l}} + \sum_{i=0}^{2n} \omega^i_c \left[y^i_{k-1,l} - \hat{y}^-_{k-1,l}\right] \left[y^i_{k-1,l} - \hat{y}^-_{k-1,l}\right]^T. \tag{39}$$

Step 10: When the microscopic time scale $l = L$, replace l in the equations from step 3 to step 7 with L:

$$x^i_{k-1,L} = \left(\hat{x}_{k-1,L}, \hat{x}_{k-1,L} + \sqrt{(n+\lambda)P_{k-1,L}}, \hat{x}_{k-1,L} - \sqrt{(n+\lambda)P_{k-1,L}}\right). \tag{40}$$

$$x_{k-1,L}^{i} = f\left(x_{k-1,L}^{i}, \hat{\theta}_{k}^{-}, u_{k-1,L}\right). \tag{41}$$

$$P_{xx} = \sum_{i=0}^{2n} \omega_{c}^{i} \left[x_{k-1,L}^{i} - \hat{x}_{k-1,L}^{-}\right] \left[x_{k-1,L}^{i} - \hat{x}_{k-1,L}^{-}\right]^{T} + Q_{k-1,L-1}. \tag{42}$$

$$x_{k-1,L}^{i} = \left(\hat{x}_{k-1,L}^{-}, \hat{x}_{k-1,L}^{-} + \sqrt{(n+\lambda)P_{xx}}, \hat{x}_{k-1,L}^{-} - \sqrt{(n+\lambda)P_{xx}}\right). \tag{43}$$

$$y_{k-1,L}^{i} = g\left(x_{k-1,L}^{i}, \hat{\theta}_{k}^{-}, u_{k-1,L}\right). \tag{44}$$

$$\hat{y}_{k-1,L}^{-} = \sum_{i=0}^{2n} \omega_{m}^{i} y_{k-1,L}^{i}. \tag{45}$$

$$P_{yy} = \sum_{i=0}^{2n} \omega_{c}^{i} \left[y_{k-1,L}^{i} - \hat{y}_{k-1,L}^{-}\right] \left[y_{k-1,L}^{i} - \hat{y}_{k-1,L}^{-}\right]^{T} + R_{k-1,L}. \tag{46}$$

$$P_{xy} = \sum_{i=0}^{2n} \omega_{c}^{i} \left[x_{k-1,L}^{i} - \hat{x}_{k-1,L}^{-}\right] \left[y_{k-1,L}^{i} - \hat{y}_{k-1,L}^{-}\right]^{T}. \tag{47}$$

$$K_{k-1,L}^{x} = P_{xy}\left(P_{yy}\right)^{-1}. \tag{48}$$

$$\hat{x}_{k-1,L} = \hat{x}_{k-1,L}^{-} + K_{k-1,L}^{x}\left(y_{k-1,L} - \hat{y}_{k-1,L}^{-}\right). \tag{49}$$

$$P_{k-1,L} = P_{xx} - K_{k-1,L}^{x} P_{xy}^{T}. \tag{50}$$

Step 11: Switch the microscopic time scale to the macroscopic time scale, where $l = 0$, denoted as

$$\hat{x}_{k,0} = \hat{x}_{k-1,L}. \tag{51}$$

$$P_{k,0} = P_{k-1,L}. \tag{52}$$

$$y_{k,0} = y_{k-1,L}. \tag{53}$$

$$u_{k,0} = u_{k-1,L}. \tag{54}$$

Step 12: Calculate the extended Kalman filter gain matrix at time k, by Equation (13).

Step 13: Adaptive update of the process noise variance matrix of the system parameter using the innovation value [32].

The innovation value at time k is expressed as

$$\begin{aligned} m_{k} &= y_{k,0} - \hat{y}_{k,0}^{-} \\ &= y_{k,0} - g\left(\hat{x}_{k,0}, \hat{\theta}_{k}^{-}, u_{k,0}\right) \end{aligned} \tag{55}$$

Calculate the real-time estimated variance value of the innovation at time k.

$$G_{m_k} = \begin{cases} \frac{k-1}{k} G_{m_{k-1}} + \frac{1}{k} m_k m_k^T & k \le N \\ \frac{1}{N} \sum\limits_{q=k-N+1}^{k} m_q m_q^T & k > N, \end{cases} \tag{56}$$

where m_q is an element value of m_k in the range $q = k - N + 1$ to k.

The process noise variance matrix of the system parameter is updated with the real-time estimated variance value of the innovation, denoted as

$$M_{k-1} = K_k^{\theta} G_{m_k} \left(K_k^{\theta}\right)^T. \tag{57}$$

Step 14: Correct the system parameter and parameter variance matrix at time k on the macroscopic time scale.

$$\hat{\theta}_k = \hat{\theta}_k^- + K_k^{\theta}\left(y_{k,0} - g\left(\hat{x}_{k,0}, \hat{\theta}_k^-, u_{k,0}\right)\right). \tag{58}$$

$$P_{\theta_k} = \left(I - K_k^{\theta} C_k^{\theta}\right) P_{\theta_k}^-. \tag{59}$$

Step 15: Adaptive update of the observed noise variance matrix of the system parameter using the residual value.

The residual value at time k is expressed as

$$r_k = y_{k,0} - \hat{y}_{k,0} = y_{k,0} - g\left(\hat{x}_{k,0}, \hat{\theta}_k, u_{k,0}\right) \tag{60}$$

Calculate the real-time estimated variance value of the residual at time k.

$$G_{r_k} = \begin{cases} \frac{k-1}{k} G_{r_{k-1}} + \frac{1}{k} r_k r_k^T & k \le N \\ \frac{1}{N} \sum\limits_{q=k-N+1}^{k} r_q r_q^T & k > N' \end{cases} \tag{61}$$

where r_q is an element value of r_k in the range $q = k - N + 1$ to k.

The observed noise variance matrix of the system parameter is updated with the real-time estimated variance value of the residual, denoted as

$$R_k = G_{r_k} + C_k^{\theta} P_k \left(C_k^{\theta}\right)^T. \tag{62}$$

Step 16: Substitute the updated system parameter $\hat{\theta}_k$ for θ_k in Equation (5), update the state space equations of the lithium-ion batteries, and perform the next round of cycle calculation for the parameter identification and SoC estimation of the lithium-ion batteries.

The flow block diagram of the multi-timescale AEKF–AUKF joint algorithm is shown in Figure 2.

4. Lithium-Ion Batteries Online Parameter Identification Algorithms Analysis

The parameter identification experiments are implemented using the second-order *RC* equivalent circuit model of the lithium-ion batteries. The AEKF algorithm used for online identification on a macroscopic time scale is carried out to obtain the model parameters R_0, R_1, C_1, R_2, and C_2, which are used for the SoC estimation of the lithium-ion batteries. In order to analyze the accuracy of the identification results, as well as the robustness and adaptiveness of the algorithm, the estimated terminal voltage can be obtained from the identified parameter values according to Equation (7) and compared with the actual terminal voltage. This algorithm is important for many applications, such as the estimation of the batteries' condition and fault diagnosis [33].

4.1. Fitting the Open-Circuit Voltage Equation Based on Measured Data

This paper studies a battery pack consisting of 10 INR18650-30Q lithium-ion batteries in parallel, with a testing environment temperature of 25 °C. The specific parameters of the batteries are shown in Table 1.

The parameter identification of a lithium-ion batteries model mainly involves two steps. The first step is to obtain the relationship between the open circuit voltage (U_{oc}) and the *SoC*through pulse discharge experiments at a constant temperature (25 °C). The second step

is to identify the relevant parameters, R_0, R_1, C_1, R_2, and C_2, of the lithium-ion batteries' equivalent circuit model online through the urban dynamometer driving schedule (UDDS).

Table 1. Parameters of lithium-ion batteries.

Parameter	Value
Batteries name	INR18650-30Q
Size	18 mm (D) × 65 mm (H)
Rated capacity	3000 mAh
Rated voltage	3.6 V
Discharge cut-off voltage	2.5 V

Use a constant pulse of 30 A to discharge the batteries at a discharge rate of 1C for 3 min, and then let it stand for 2 h. Cycle the discharge to the cut-off voltage and record the open circuit voltage value of the batteries during this process. The pulse discharge current and voltage are shown in Figure 3.

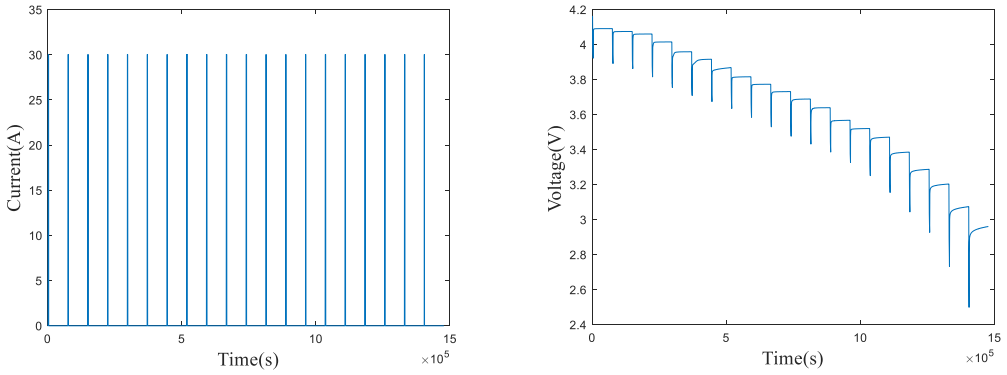

(**a**) (**b**)

Figure 3. Current and voltage curves for pulse discharge condition: (**a**) pulse discharge current; (**b**) pulse discharge voltage.

Based on the experimental data of the open circuit voltage of lithium-ion batteries, the curve fitting toolbox in MATLAB was used to perform a ninth-order fitting on the functional relationship equation between U_{oc} and SoC, and the equation was obtained as follows

$$\begin{aligned} U_{oc}(SoC) &= p(1)SoC^9 + p(2)SoC^8 + p(3)SoC^7 \\ &+ p(4)SoC^6 + p(5)SoC^5 + p(6)SoC^4 \\ &+ p(7)SoC^3 + p(8)SoC^2 + p(9)SoC + p(10). \end{aligned} \tag{63}$$

The U_{oc} (SoC) equation curve is shown in Figure 4.

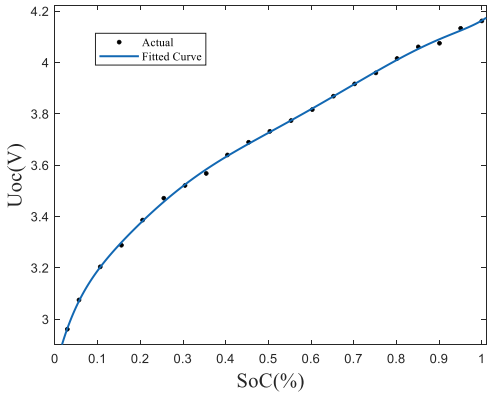

Figure 4. U_{oc} (SoC) equation curve.

4.2. Online Identification of Lithium-Ion Batteries Parameters Based on the AEKF Algorithm

In this paper, the UDDS condition is used as the actual condition for the online identification of lithium-ion batteries' parameters. The current and voltage under the UDDS condition are shown in Figure 5.

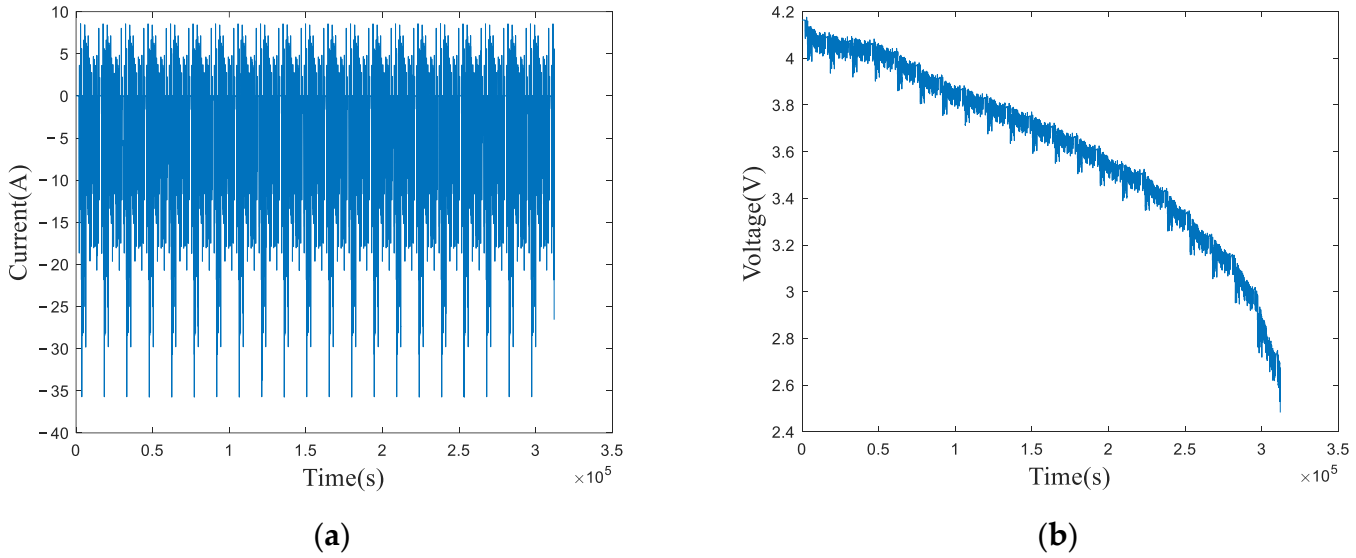

Figure 5. UDDS operating current and voltage curves: (**a**) UDDS operating current; (**b**) UDDS opreating voltage.

In this paper, the AEKF algorithm is used in combination with Equation (63) to identify the parameters of the second-order *RC* equivalent circuit of lithium-ion batteries under UDDS conditions online. The parameter identification results of R_0, R_1, R_2, C_1, and C_2 are obtained, as shown in Figures 6 and 7.

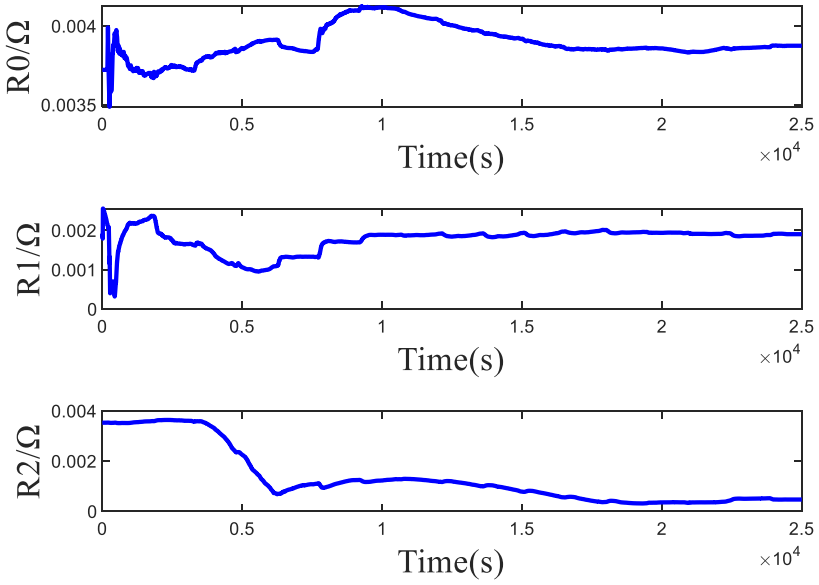

Figure 6. R_0, R_1, and R_2 parameter identification results.

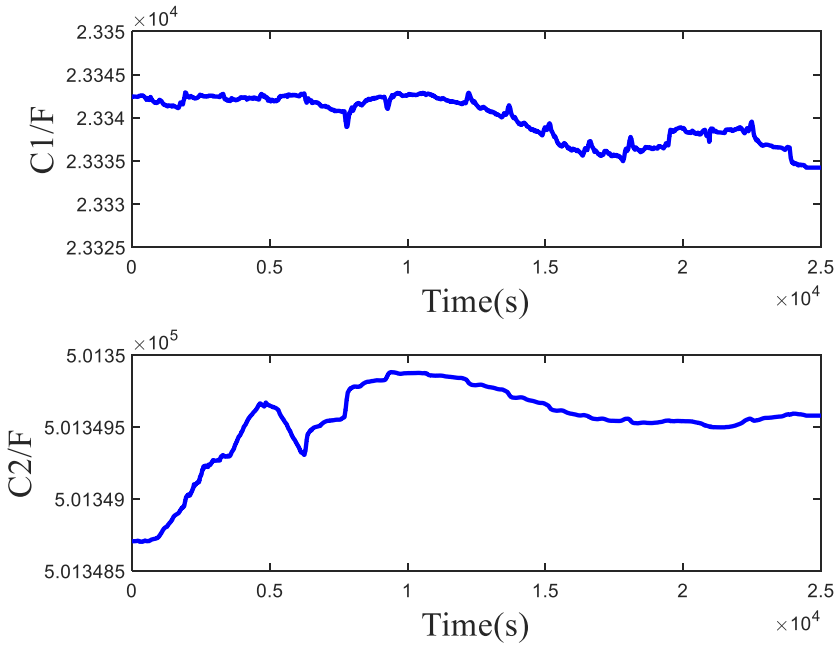

Figure 7. C_1 and C_2 parameter identification results.

In the early stage of the online parameter identification process, the changes of R_0, R_1, and R_2 are relatively drastic, which is mainly due to the imprecise selection of the initial values of the model; the fluctuations of the time constants τ_1 and τ_2 are not large, and the value of τ_1 is much smaller than the value of τ_2.

4.3. Accuracy Analysis of Online Identification Algorithm for Lithium-Ion Batteries' Parameters

For comparison, the EKF algorithm and AEKF algorithm are respectively used for online parameter identification of the second-order *RC* equivalent circuit model at the macro time scale. This paper uses terminal voltage errors to compare the accuracy, robustness, and adaptability of the two algorithms. The comparison curves of terminal voltage errors are shown in Figure 8.

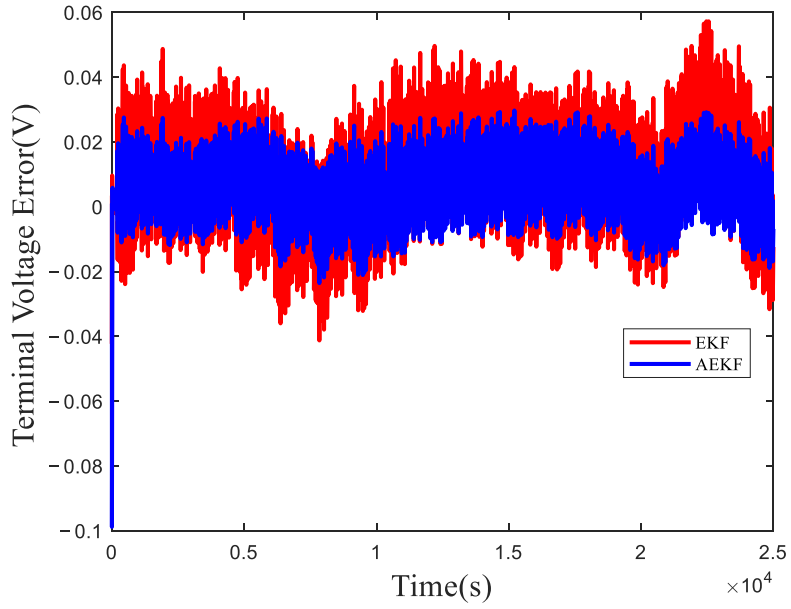

Figure 8. Terminal voltage error curves.

According to Figure 8, the mean absolute error (MAE) of the model terminal voltage is 0.0075 and the root mean square error (RMSE) is 0.0095 after online parameter identification using the EKF algorithm, while the MAE of the model terminal voltage is 0.0042 and the RMSE is 0.0052 after online parameter identification using the AEKF algorithm, as shown in Table 2.

Table 2. Comparison of terminal voltage errors between the EKF algorithm and the AEKF algorithm.

Online Parameter Identification Algorithm	MAE	RMSE
EKF	0.0075	0.0095
AEKF	0.0042	0.0052

By comparing and analyzing the terminal voltage errors of the two algorithms, it is shown that the AEKF algorithm has higher identification efficiency and smaller terminal voltage errors and fluctuations, indicating that the AEKF algorithm has good parameter identification accuracy, strong robustness, and adaptability under complex working conditions.

5. Lithium-Ion Batteries SoC Estimation Algorithm Analysis

5.1. Case I: Estimation Accuracy Analysis of Multi-Timescale Algorithm

In order to improve the accuracy of parameter identification and SoC estimation of lithium-ion batteries, the multi-timescale AEKF–AUKF joint algorithm is used as L = 60 s, which considers multiple time scale algorithms.

The AEKF algorithm is used for online parameter identification at the macroscopic time scale, and the AUKF algorithm is used for SoC estimation at the microscopic time scale. The terminal voltage and SoC estimation results of the lithium-ion batteries are shown in Figure 9.

The comparison curves between the actual and estimated terminal voltage are shown in Figure 9a, the terminal voltage estimation error is shown in Figure 9b, the comparison curves between the actual SoC and the estimated SoC are shown in Figure 9c, and the SoC estimation error is shown in Figure 9d.

When L = 60 s, the MAE of the terminal voltage under the multi-timescale AEKF–AUKF joint algorithm is 0.0042 and the RMSE is 0.0052, and the MAE of the SoC estimation is 0.0034 and the RMSE is 0.0043. Based on the analysis of the estimation results of the multi-timescale AEKF–AUKF joint algorithm, it can be concluded that both the estimated terminal voltage and the estimated SoC value under this joint algorithm have very small differences from the actual values; therefore, it can be judged that the joint algorithm calculation results are accurate and valid.

In order to more comprehensively analyze the performance of the estimation results under the multi-timescale AEKF–AUKF joint algorithm, the following three cases were set up to compare and analyze the estimation accuracy of terminal voltage and SoC under UDDS conditions with various algorithms.

5.2. Case II: Analysis of the Effect of Time Scale on Estimation Accuracy

When L = 1 s, the AEKF–AUKF joint algorithm can be used for online parameter identification and SoC estimation of lithium-ion batteries without considering multiple time scales. Figure 10 shows a comparison of two simulation results for L = 1 s and L = 60 s.

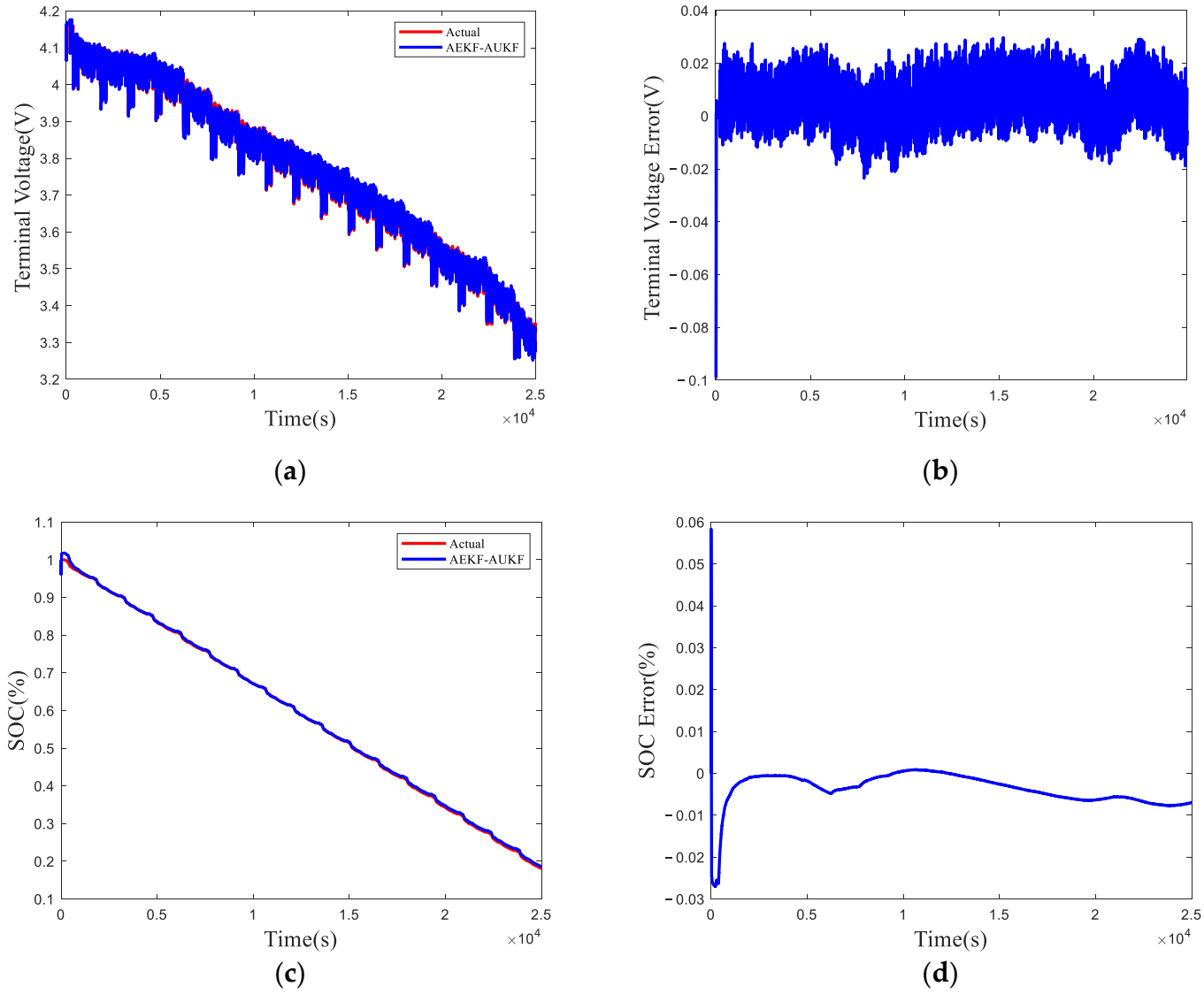

Figure 9. Results of the multi-timescale AEKF–AUKF joint algorithm: (**a**) comparison curves between the actual and estimated terminal voltage; (**b**) terminal voltage estimation error; (**c**) comparison curves between the actual and estimated SoC; (**d**) SoC estimation error.

The comparison curves between the actual and estimated terminal voltage are shown in Figure 10a, the comparison curves of the terminal voltage estimation error are shown in Figure 10b, the comparison curves between the actual SoC and the estimated SoC are shown in Figure 10c, and the comparison curves of the SoC estimation error are shown in Figure 10d.

As shown in Figure 10, it can be observed that the MAE of the terminal voltage is 0.0090 and the RMSE is 0.0109 when L = 1 s, and the MAE of the SoC estimation is 0.0085 and the RMSE is 0.0103, as shown in Table 3.

Table 3. Comparison of the terminal voltage and SoC estimation errors by different time scales.

	Terminal Voltage Error		**SoC Estimation Error**	
AEKF-AUKF	MAE	RMSE	MAE	RMSE
L = 1 s	0.0090	0.0109	0.0085	0.0103
L = 60 s	0.0042	0.0052	0.0034	0.0043

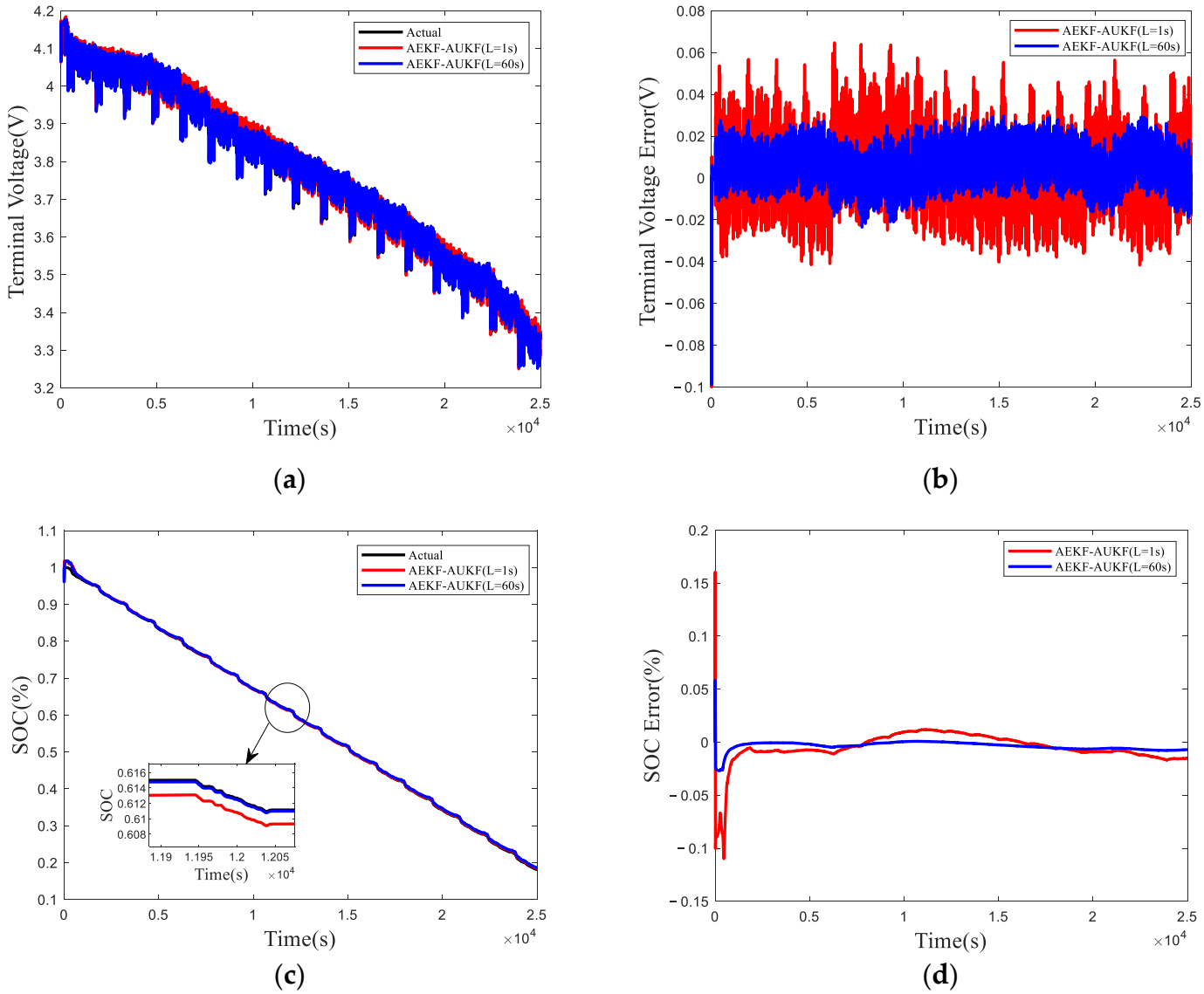

Figure 10. Results of the AEKF–AUKF joint algorithm at L = 1 s versus L = 60 s: (**a**) comparison curves between the actual and estimated terminal voltage; (**b**) comparison curves of the terminal voltage estimation error; (**c**) comparison curves between the actual and estimated SoC; (**d**) comparison curves of the SoC estimation error.

The results show that both the terminal voltage estimation error and the SoC estimation error of the AEKF–AUKF joint algorithm at L = 60 s are smaller than those at L = 1 s, and the error curve fluctuates less and is closer to the actual value. The estimation results have higher accuracy, which shows that considering multiple time scales can greatly improve the estimation accuracy and performance.

5.3. Case III: Analysis of the Effect of External Noise on Estimation Accuracy

Three joint algorithms, EKF–UKF, AEKF–UKF, and AEKF–AUKF, are used for the online parameter identification and SoC estimation of the lithium-ion batteries at multiple time scales. A comparison of the terminal voltage and SoC estimation results of the lithium-ion batteries under the three joint algorithms is shown in Figure 11.

The comparison curves between the actual and estimated terminal voltage under the three joint algorithms are shown in Figure 11a, the comparison curves of the terminal voltage estimation error are shown in Figure 11b, the comparison curves between the actual

SoC and the estimated SoC are shown in Figure 11c, and the comparison curves of the SoC estimation error are shown in Figure 11d.

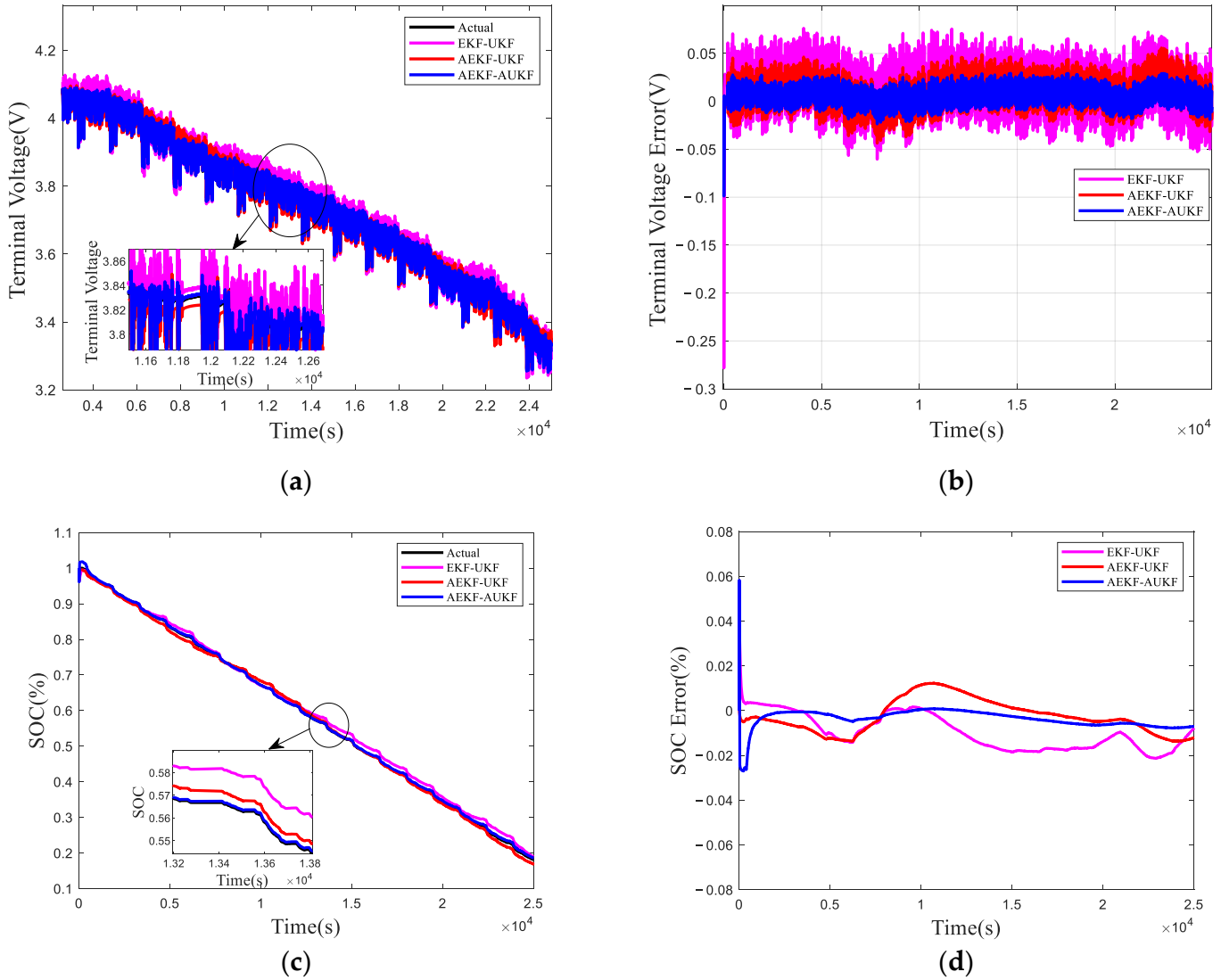

Figure 11. Comparison of the results of the three joint algorithms at multiple time scales: (**a**) comparison curves between the actual and estimated terminal voltage; (**b**) comparison curves of the terminal voltage estimation error; (**c**) comparison curves between the actual and estimated SoC; (**d**) comparison curves of the SoC estimation error.

As shown in Figure 11, the MAE of the EKF–UKF joint algorithm for the terminal voltage is 0.0086, the RMSE is 0.0118, the MAE of the SoC estimation is 0.0105, and the RMSE is 0.0125; the MAE of the AEKF–UKF joint algorithm for the terminal voltage is 0.0077, the RMSE is 0.0098, the MAE of the SoC estimation is 0.0068, and the RMSE is 0.0079, as shown in Table 4.

Table 4. Comparison of the three joint algorithms terminal voltage and SoC estimation errors.

	Terminal Voltage Error		**SoC Estimation Error**	
Joint algorithm	MAE	RMSE	MAE	RMSE
EKF–UKF	0.0086	0.0118	0.0105	0.0125
AEKF–UKF	0.0077	0.0098	0.0068	0.0079
AEKF–AUKF	0.0042	0.0052	0.0034	0.0043

From Table 4, it can be seen that due to the consideration of the uncertainty of noise and real-time correction of noise variance, the proposed AEKF–AUKF joint algorithm has smaller errors in its terminal voltage estimation and SoC estimation compared to the EKF–UKF and AEKF–UKF joint algorithms. In addition, the terminal voltage estimation error and SoC estimation error using the AEKF–UKF joint algorithm are also smaller than those using the EKF–UKF joint algorithm.

Overall, the AEKF–AUKF joint algorithm has the highest estimation accuracy, is the most suitable for actual values, and has strong adaptability. The AEKF–UKF joint algorithm has poorer estimation accuracy, and the EKF–UKF joint algorithm has the worst estimation accuracy. This illustrates that the traditional algorithm does not fully consider the uncertainty of noise and cannot truly reflect the dynamic characteristics of the noise, while the addition of the adaptive algorithm processing to the external noise can greatly reduce the influence of the external noise on the estimation accuracy and improve the adaptiveness of the algorithm.

5.4. Case IV: Analysis of the Effect of Initial Values on Estimation Accuracy

In the case of inaccurate initial values of SoC, the algorithm was analyzed for its stability in correcting the offset between the actual and estimated values of SoC, and for its ability to self-correct by converging to the actual value. The performance of the multi-timescale AEKF–AUKF joint algorithm is analyzed below at initial values of SoC = 80% and SoC = 60%, respectively, and the results are shown in Figures 12 and 13.

For the initial value of SoC = 80%, the comparison curves between the actual and estimated terminal voltage are shown in Figure 12a, the terminal voltage estimation error is shown in Figure 12b, the comparison curves between the actual SoC and the estimated SoC are shown in Figure 12c, and the SoC estimation error is shown in Figure 12d; for the initial value of SoC = 60%, the comparison curves between the actual and estimated terminal voltage are shown in Figure 13a, the terminal voltage error is shown in Figure 13b, the comparison curves between the actual SoC and the estimated SoC are shown in Figure 13c, and the SoC estimation error is shown in Figure 13d.

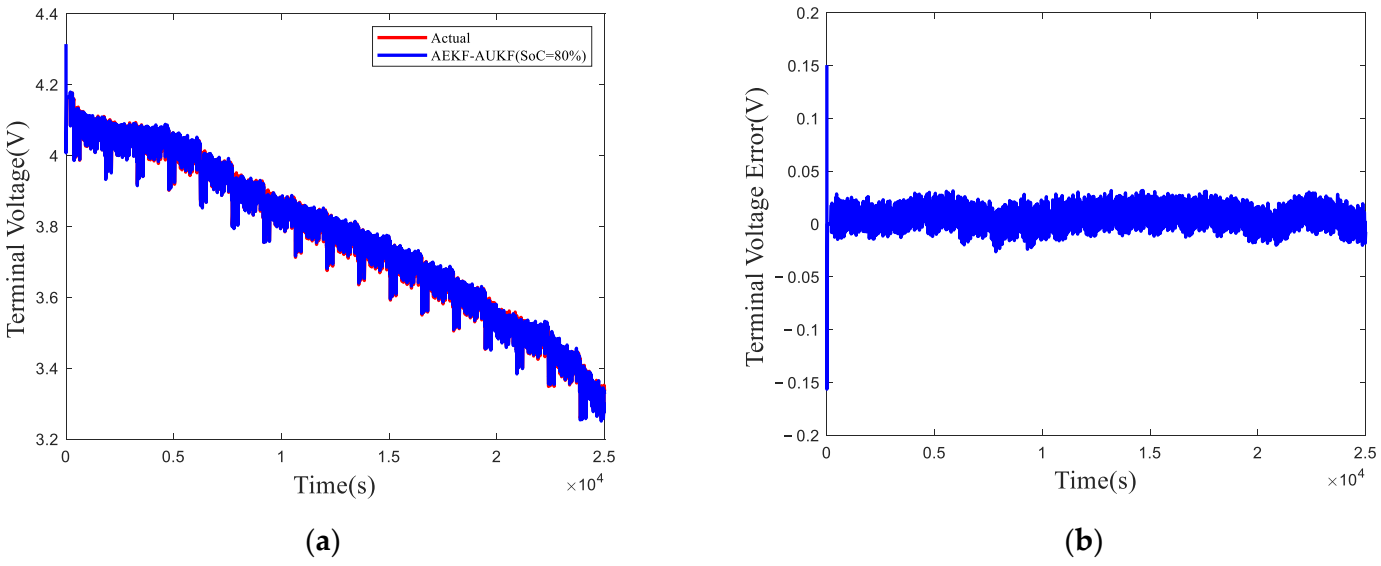

(**a**) (**b**)

Figure 12. *Cont.*

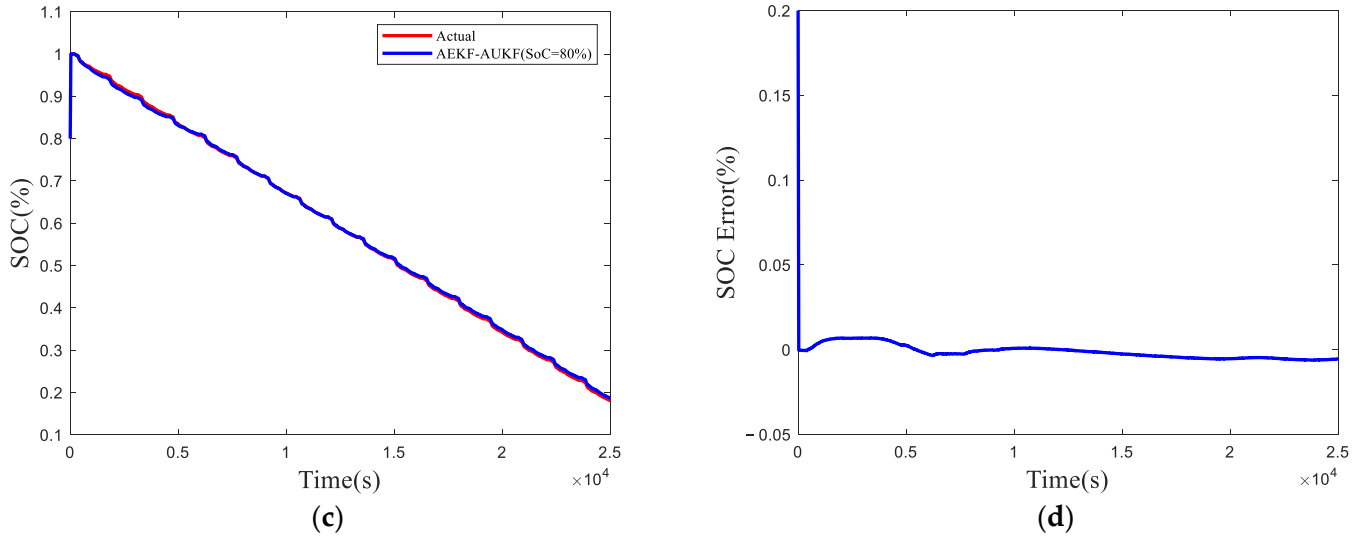

Figure 12. Results of the multi-timescale AEKF–AUKF joint algorithm at SoC = 80%: (**a**) comparison curves between the actual and estimated terminal voltage; (**b**) terminal voltage estimation error; (**c**) comparison curves between the actual and estimated SoC; (**d**) SoC estimation error.

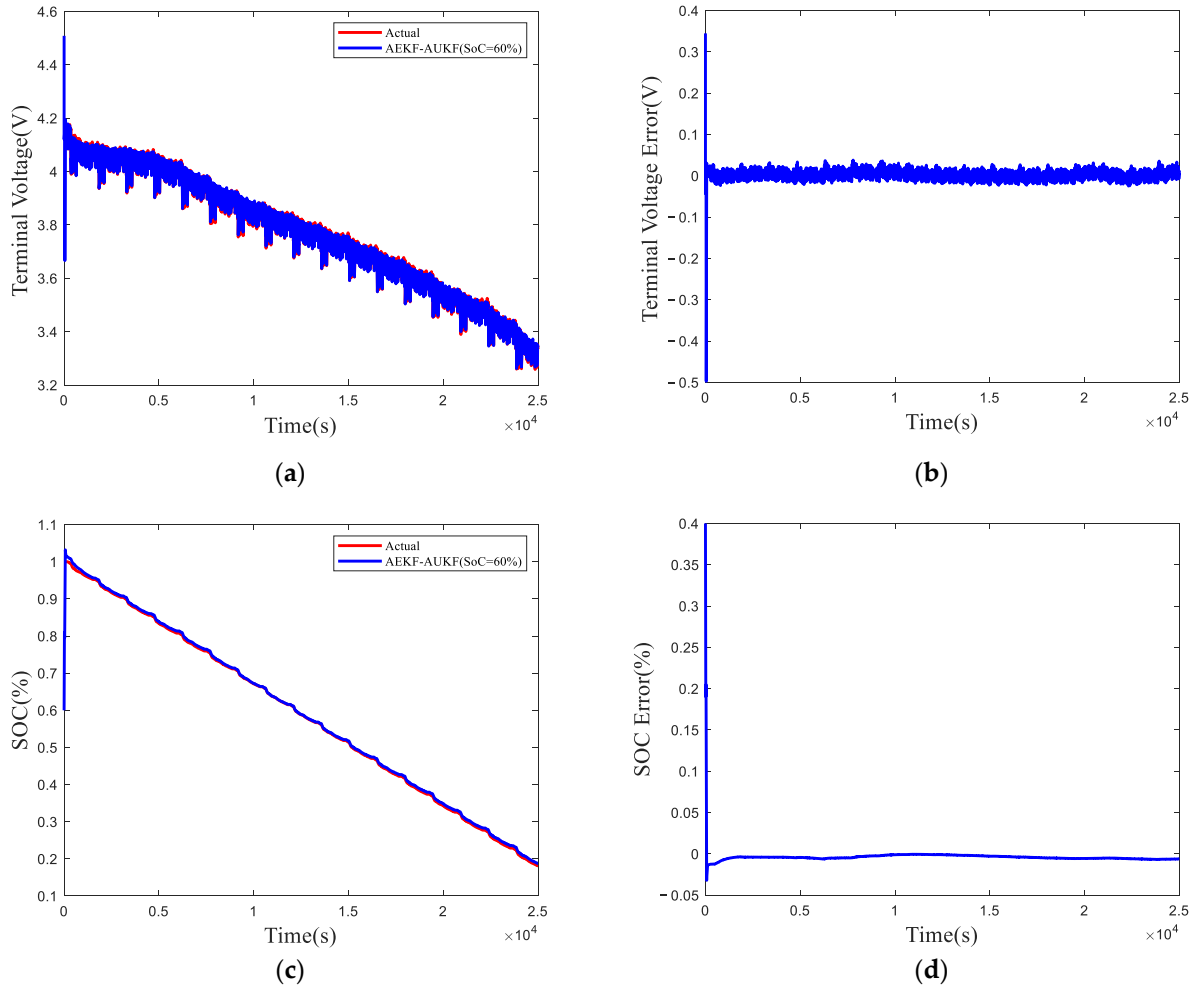

Figure 13. Results of the multi-timescale AEKF–AUKF joint algorithm at SoC = 60%: (**a**) comparison curves between the actual and estimated terminal voltage; (**b**) terminal voltage estimation error; (**c**) comparison curves between the actual and estimated SoC; (**d**) SoC estimation error.

Comparing the result plots for the initial values of SoC = 80% and SoC = 60%, the analysis of the data shows that for SoC = 80%, the MAE of the multi-timescale AEKF–AUKF joint algorithm for the terminal voltage is 0.0045, the RMSE is 0.0057, the MAE of the SoC estimation is 0.0035, and the RMSE is 0.0041; for SoC = 60%, the MAE of the multi-timescale AEKF–AUKF joint algorithm for the terminal voltage is 0.0048, the RMSE is 0.0060, the MAE of SoC estimation is 0.0041, and the RMSE is 0.0045, as shown in Table 5.

Table 5. Analysis of terminal voltage and SoC estimation errors for different SoC initial values.

	Terminal Voltage Error		**SoC Estimation Error**	
SoC value	MAE	RMSE	MAE	RMSE
SoC = 80%	0.0045	0.0057	0.0035	0.0041
SoC = 60%	0.0048	0.0060	0.0041	0.0045

The results show that for inaccurate initial SoC values, the multi-timescale AEKF–AUKF joint algorithm is able to converge steadily to near the actual value, and both the terminal voltage estimation error and the SoC estimation error are small. The error curves' fluctuations are also small, indicating that the multi-timescale AEKF–AUKF joint algorithm is able to achieve self-correction and has strong robustness.

6. Conclusions

In this paper, a multi-timescale AEKF–AUKF joint algorithm is proposed for SoC estimation of lithium-ion batteries at multiple time scales, due to the slow-varying characteristics of lithium-ion batteries model parameters and the fast-varying characteristics of SoC. The AEKF algorithm is used for online parameter identification at the macroscopic time scale, and the AUKF algorithm is used for SoC estimation at the microscopic time scale. This algorithm can quickly iterate to correct incorrect initial estimates, achieving a peak voltage error of less than 0.16% in the parameter identification process and an absolute peak SoC estimation error of less than 1.1%. This joint algorithm not only effectively improves the noise problem in SoC estimation by lithium-ion batteries, but also improves the accuracy of parameter identification and SoC estimation.

In order to analyze the estimation performance of the proposed multi-timescale AEKF–AUKF joint algorithm, three simulations have been implemented under UDDS conditions, and the parameter identification and SoC estimation results under three different algorithms have been compared and analyzed. The results show that the following: (1) the AEKF–AUKF joint algorithm greatly improves the estimation accuracy of the lithium-ion batteries' SoC when multiple time scales are considered; (2) the multi-timescale AEKF–AUKF joint algorithm enables real-time correction of external noise in the lithium-ion batteries under complex operating conditions, improving the adaptiveness of SoC estimation of lithium-ion batteries; (3) when the initial SoC estimation value is inaccurate, the multi-timescale AEKF–AUKF joint algorithm can stably correct the offset and converge to the reference value, with self-correction capability, improving the robustness of SoC estimation of lithium-ion batteries.

The algorithm has the advantages of simplicity, ease of use, and high accuracy, and can be applied to real-time estimation and monitoring of the SoC of lithium-ion batteries.

Author Contributions: Conceptualization, A.W. and Y.Z.; methodology, Y.Z. and J.M.; software, Y.Z. and J.M.; validation, A.W., Y.Z. and J.M.; formal analysis, X.Z. and J.Z.; investigation, A.W. and J.M.; resources, X.Z.; data curation, J.M. and J.Z.; writing—original draft preparation, Y.Z.; writing—review and editing, J.M.; supervision, A.W. and J.M.; project administration, J.M.; funding acquisition, J.M. All authors have read and agreed to the published version of the manuscript.

Funding: This work is financially supported in part by the Natural Science Research Program of Jiangsu Colleges and Universities under Grant No. 20KJA470002, and the Excellent Teaching Team of the "Qinglan Project" of Jiangsu Colleges and Universities.

Data Availability Statement: Not applicable.

Conflicts of Interest: The authors declare no conflict of interest.

References

1. Hannan, M.A.; Lipu, M.S.H.; Hussain, A.; Mohamed, A. A Review of Lithium-Ion Battery State of Charge Estimation and Management System in Electric Vehicle Applications: Challenges and Recommendations. *Renew. Sustain. Energy Rev.* **2017**, *78*, 834–854. [CrossRef]
2. Xie, Y.; Li, W.; Hu, X.; Tran, M.-K.; Panchal, S.; Fowler, M.; Zhang, Y.; Liu, K. Coestimation of SOC and Three-Dimensional SOT for Lithium-Ion Batteries Based on Distributed Spatial–Temporal Online Correction. *IEEE Trans. Ind. Electron.* **2023**, *70*, 5937–5948. [CrossRef]
3. How, D.N.T.; Hannan, M.A.; Hossain Lipu, M.S.; Ker, P.J. State of Charge Estimation for Lithium-Ion Batteries Using Model-Based and Data-Driven Methods: A Review. *IEEE Access* **2019**, *7*, 136116–136136. [CrossRef]
4. Lu, L.; Han, X.; Li, J.; Hua, J.; Ouyang, M. A Review on the Key Issues for Lithium-Ion Battery Management in Electric Vehicles. *J. Power Source* **2013**, *226*, 272–288. [CrossRef]
5. Chen, J.; Ouyang, Q.; Xu, C.; Su, H. Neural Network-Based State of Charge Observer Design for Lithium-Ion Batteries. *IEEE Trans. Contr. Syst. Technol.* **2018**, *26*, 313–320. [CrossRef]
6. Li, J.; Ye, M.; Meng, W.; Xu, X.; Jiao, S. A Novel State of Charge Approach of Lithium Ion Battery Using Least Squares Support Vector Machine. *IEEE Access* **2020**, *8*, 195398–195410. [CrossRef]
7. Salazar, D.; Garcia, M. Estimation and Comparison of SOC in Batteries Used in Electromobility Using the Thevenin Model and Coulomb Ampere Counting. *Energies* **2022**, *15*, 7204. [CrossRef]
8. Chen, X.; Lei, H.; Xiong, R.; Shen, W.; Yang, R. A Novel Approach to Reconstruct Open Circuit Voltage for State of Charge Estimation of Lithium Ion Batteries in Electric Vehicles. *Appl. Energy* **2019**, *255*, 113758. [CrossRef]
9. Yang, B.; Li, G.; Tang, W.; Li, H. Research on Optimized SOC Estimation Algorithm Based on Extended Kalman Filter. *Front. Energy Res.* **2022**, *10*, 1027439. [CrossRef]
10. Miao, Y.; Gao, Z.; Xiao, S.; Chai, H. Initial Value Compensation of an Adaptive Fractional-Order Unscented Kalman Filter for Estimating the State of Charge of Lithium-Ion Batteries. *J. Energy Storage* **2023**, *70*, 107857. [CrossRef]
11. Ma, W.; Guo, P.; Wang, X.; Zhang, Z.; Peng, S.; Chen, B. Robust State of Charge Estimation for Li-Ion Batteries Based on Cubature Kalman Filter with Generalized Maximum Correntropy Criterion. *Energy* **2022**, *260*, 125083. [CrossRef]
12. Zhu, R.; Duan, B.; Zhang, J.; Zhang, Q.; Zhang, C. Co-Estimation of Model Parameters and State-of-Charge for Lithium-Ion Batteries with Recursive Restricted Total Least Squares and Unscented Kalman Filter. *Appl. Energy* **2020**, *277*, 115494. [CrossRef]
13. Ge, C.; Zheng, Y.; Yu, Y. State of Charge Estimation of Lithium-Ion Battery Based on Improved Forgetting Factor Recursive Least Squares-Extended Kalman Filter Joint Algorithm. *J. Energy Storage* **2022**, *55*, 105474. [CrossRef]
14. Wu, C.; Hu, W.; Meng, J.; Xu, X.; Huang, X.; Cai, L. State-of-Charge Estimation of Lithium-Ion Batteries Based on MCC-AEKF in Non-Gaussian Noise Environment. *Energy* **2023**, *274*, 127316. [CrossRef]
15. Liu, G.; Xu, C.; Li, H.; Jiang, K.; Wang, K. State of Charge and Online Model Parameters Co-Estimation for Liquid Metal Batteries. *Appl. Energy* **2019**, *250*, 677–684. [CrossRef]
16. Xiong, R.; Sun, F.; Chen, Z.; He, H. A Data-Driven Multi-Scale Extended Kalman Filtering Based Parameter and State Estimation Approach of Lithium-Ion Polymer Battery in Electric Vehicles. *Appl. Energy* **2014**, *113*, 463–476. [CrossRef]
17. Ji, S.; Sun, Y.; Chen, Z.; Liao, W. A Multi-Scale Time Method for the State of Charge and Parameter Estimation of Lithium-Ion Batteries Using MIUKF-EKF. *Front. Energy Res.* **2022**, *10*, 933240. [CrossRef]
18. Feng, F.; Song, B.; Xu, J.; Na, W.; Zhang, K.; Chai, Y. Multiple Time Scale State-of-Charge and Capacity-Based Equalisation Strategy for Lithium-Ion Battery Pack with Passive Equaliser. *J. Energy Storage* **2022**, *53*, 105196. [CrossRef]
19. Fajri, P.; Ferdowsi, M.; Lotfi, N.; Landers, R. Development of an Educational Small-Scale Hybrid Electric Vehicle (HEV) Setup. *IEEE Intell. Transport. Syst. Mag.* **2016**, *8*, 8–21. [CrossRef]
20. Duan, W.; Song, C.; Chen, Y.; Xiao, F.; Peng, S.; Shao, Y.; Song, S. Online Parameter Identification and State of Charge Estimation of Battery Based on Multitimescale Adaptive Double Kalman Filter Algorithm. *Math. Probl. Eng.* **2020**, *2020*, 1–20. [CrossRef]
21. Huang, J.; An, H.; Lang, L.; Wei, Q.; Ma, H. A Data-Driven Multi-Scale Online Joint Estimation of States and Parameters for Electro-Hydraulic Actuator in Legged Robot. *IEEE Access* **2020**, *8*, 36885–36902. [CrossRef]
22. Huang, Z.; Fang, Y.; Xu, J. SOC Estimation of Li-ION Battery Based on Improved EKF Algorithm. *Int. J. Automot. Technol.* **2021**, *22*, 335–340. [CrossRef]
23. Peng, X.; Li, Y.; Yang, W.; Garg, A. Real-Time State of Charge Estimation of the Extended Kalman Filter and Unscented Kalman Filter Algorithms Under Different Working Conditions. *J. Electrochem. Energy Convers. Storage* **2021**, *18*, 041007. [CrossRef]
24. Hu, G.; Gao, B.; Zhong, Y.; Gu, C. Unscented Kalman Filter with Process Noise Covariance Estimation for Vehicular Ins/Gps Integration System. *Inf. Fusion* **2020**, *64*, 194–204. [CrossRef]
25. Peng, N.; Zhang, S.; Guo, X.; Zhang, X. Online Parameters Identification and State of Charge Estimation for Lithium-ion Batteries Using Improved Adaptive Dual Unscented Kalman Filter. *Int. J. Energy Res.* **2021**, *45*, 975–990. [CrossRef]
26. Ding, H.; Qin, X.; Wei, L. Sensorless Control of Surface-Mounted Permanent Magnet Synchronous Motor Using Adaptive Robust UKF. *J. Electr. Eng. Technol.* **2022**, *17*, 2995–3013. [CrossRef]

27. Ge, B.; Zhang, H.; Jiang, L.; Li, Z.; Butt, M. Adaptive Unscented Kalman Filter for Target Tracking with Unknown Time-Varying Noise Covariance. *Sensors* **2019**, *19*, 1371. [CrossRef] [PubMed]
28. Plett, G.L. Extended Kalman Filtering for Battery Management Systems of LiPB-Based HEV Battery Packs. *J. Power Source* **2004**, *134*, 277–292. [CrossRef]
29. Zhou, Y.; Wang, S.; Xie, Y.; Zhu, T.; Fernandez, C. An Improved Particle Swarm Optimization-Least Squares Support Vector Machine-Unscented Kalman Filtering Algorithm on SOC Estimation of Lithium-Ion Battery. *Int. J. Green Energy* **2023**, 1–11. [CrossRef]
30. Zhang, Q.; Yang, Y.; Xiang, Q.; He, Q.; Zhou, Z.; Yao, Y. Noise Adaptive Kalman Filter for Joint Polarization Tracking and Channel Equalization Using Cascaded Covariance Matching. *IEEE Photonics J.* **2018**, *10*, 7900911. [CrossRef]
31. Song, M.; Astroza, R.; Ebrahimian, H.; Moaveni, B.; Papadimitriou, C. Adaptive Kalman Filters for Nonlinear Finite Element Model Updating. *Mech. Syst. Signal Process.* **2020**, *143*, 106837. [CrossRef]
32. Xu, Y.; Hu, B.; Wu, T.; Zhou, X.; Xiao, T. The Multi-Innovation Adaptive Extended Kalman Filter Algorithm for Battery SOC Estimation. In Proceedings of the 2021 4th International Conference on Advanced Electronic Materials, Computers and Software Engineering (AEMCSE), Changsha, China, 26–28 March 2021; IEEE: Changsha, China, 2021; pp. 159–166.
33. Sadhukhan, C.; Mitra, S.K.; Bhattacharyya, S.; Almatrafi, E.; Saleh, B.; Naskar, M.K. Modeling and Simulation of High Energy Density Lithium-Ion Battery for Multiple Fault Detection. *Sci. Rep.* **2022**, *12*, 9800. [CrossRef] [PubMed]